Structural changes in senescing oilseed rape leaves at tissue and subcellular levels monitored by nuclear magnetic resonance relaxometry through water status

Maja Musse, Loriane de Franceschi, Mireille Cambert, Clement Sorin, Françoise Le Cahérec, Agnès Burel, Alain Bouchereau, Francois Mariette, Laurent Leport

Structural Changes in Senescing Oilseed Rape Leaves at Tissue and Subcellular Levels Monitored by Nuclear Magnetic Resonance Relaxometry through Water Status

Maja Musse, Loriane De Franceschi, Mireille Cambert, Clément Sorin, Françoise Le Caherec, Agnès Burel, Alain Bouchereau, François Mariette, and Laurent Leport*

Institut National de Recherche en Sciences et Technologies pour l'Environnement et l'Agriculture, Food Process Engineering Research Unit, F–35044 Rennes cedex, France (M.M., L.D.F., M.C., C.S., F.M.); Université Européenne de Bretagne, 5 Boulevard Laënnec, 35000 Rennes, France (M.M., L.D.F., M.C., C.S., F.L.C., A.Bu., A.Bo., F.M., L.L.); INRA, UMR 1349, Institute for Genetics, Environment and Plant Protection (IGEPP), UMR INRA-Agrocampus Ouest-Université de Rennes 1, 35653 Le Rheu cedex, France (L.D.F., C.S., F.L.C., A.Bo., L.L.); and Microscopy, Rennes Imaging Center, Faculté de Médecine, CS 34317 Rennes cedex, France (A.Bu.)

ORCID ID: 0000-0001-9886-287X (L.L.).

Nitrogen use efficiency is relatively low in oilseed rape (*Brassica napus*) due to weak nitrogen remobilization during leaf senescence. Monitoring the kinetics of water distribution associated with the reorganization of cell structures, therefore, would be valuable to improve the characterization of nutrient recycling in leaf tissues and the associated senescence processes. In this study, nuclear magnetic resonance (NMR) relaxometry was used to describe water distribution and status at the cellular level in different leaf ranks of well-watered plants. It was shown to be able to detect slight variations in the evolution of senescence. The NMR results were linked to physiological characterization of the leaves and to light and electron micrographs. A relationship between cell hydration and leaf senescence was revealed and associated with changes in the NMR signal. The relative intensities and the transverse relaxation times of the NMR signal components associated with vacuole water were positively correlated with senescence, describing water uptake and vacuole and cell enlargement. Moreover, the relative intensity of the NMR signal that we assigned to the chloroplast water decreased during the senescence process, in agreement with the decrease in relative chloroplast volume estimated from micrographs. The results are discussed on the basis of water flux occurring at the cellular level during senescence. One of the main applications of this study would be for plant phenotyping, especially for plants under environmental stress such as nitrogen starvation.

The main physiological outcome of leaf senescence is the recycling of organic resources and the provision of nutrients to sink organs such as storage and growing tissues (Buchanan-Wollaston, 1997; Hikosaka, 2005; Krupinska and Humbeck, 2008). In crop plants, senescence progresses from the lower older leaves to the younger top leaves. Macromolecular degradation and the mechanism of reallocation of breakdown products are mediated by the up-regulation of senescence-related genes (Lee et al., 2001) in close relationship with both developmental and environmental conditions (Gombert et al., 2006). This leads to remobilization of carbon and nitrogen (N) compounds mostly from plastidial compartments (Martínez et al., 2008; Guiboileau et al., 2012), involving proteolytic activity in plasts, vacuole, and cytosol (Adam and Clarke, 2002; Otegui et al., 2005), chlorophyll breakdown (Hoertensteiner, 2006), galactolipid recycling (Kaup et al., 2002) in the plastoglobules (Brehelin et al., 2007), and loading of Suc and amino acids into the phloem through appropriate transporters (Wingler et al., 2004; Masclaux-Daubresse et al., 2008). In terms of leaf senescence at the cell level, where chloroplasts are degraded sequentially, relative organelle volume does not seem to be greatly modified, the vacuole remains intact, and in darkness-induced senescence the number of chloroplasts per cell decreases only slightly (Keech et al., 2007). However, major changes in metabolic fluxes and cell water relationships are expected during the senescence program that may be associated with macromolecule catabolism, organic solute synthesis, transport and remobilization, and cell structure reconfiguration such as chloroplast evolution to gerontoplast (Hoertensteiner, 2006; Zhang et al., 2010) through the autophagy process (Wada et al., 2009), accumulation of senescence-associated vacuoles (Otegui et al., 2005), and cell wall degradation (Mohapatra et al., 2010).

The senescent leaves of oilseed rape (*Brassica napus*), a major oleiferous crop, generally fall while still maintaining a high N content (about 2.5%–3% [w/w] of the dry matter; Malagoli et al., 2005). In addition to the environmental impact of this leaking of N out of the plant, the low capacity to remobilize foliar N is associated with a high requirement for N fertilization to meet

* Address correspondence to laurent.leport@univ-rennes1.fr.

The author responsible for distribution of materials integral to the findings presented in this article in accordance with the policy described in the Instructions for Authors (www.plantphysiol.org) is: Laurent Leport (laurent.leport@univ-rennes1.fr).

www.plantphysiol.org/cgi/doi/10.1104/pp.113.223123

the potential crop yield (Dreccer et al., 2000). In order to improve the nitrogen use efficiency (NUE), new genotypes are being selected for their ability to maintain high yields under limited N fertilization, mainly via the improvement of N uptake efficiency and N mobilization from the senescing leaves (Hirel et al., 2007). In Arabidopsis (*Arabidopsis thaliana*) and oilseed rape, N can be remobilized from old to expanding leaves at the vegetative stage during sequential senescence as well as from leaves to seeds at the reproductive stage during monocarpic senescence (Malagoli et al., 2005; Diaz et al., 2008; Lemaitre et al., 2008). Senescence can also be induced by environmental stress such as N starvation (Etienne et al., 2007) or water deficit (Reviron et al., 1992) and propagated from old to mature leaves and delayed in young leaves, suggesting finely tuned high regulation of metabolism at the whole-plant level with consequences for NUE (Desclos et al., 2008). One major challenge to understanding the efficiency of senescence-induced organic resource reallocation and to highlighting major molecular and mechanistic attributes of nutrient recycling is monitoring the kinetics of the structural reorganization of cell structures. This reorganization will provide nutrients remobilized through phloem loading. From a technological and phenotyping point of view, the measurement of N remobilization efficiency has already been addressed in crop species and oilseed rape, as it is a reliable trait to screen for the genetic variability of NUE (Franzaring et al., 2012). However, techniques such as stable isotope feeding are time consuming, destructive, and difficult to adapt to large genotype panels. Therefore, it is important to develop a technique for following changes in water distribution at the cell level in order to understand metabolic reconfigurations occurring throughout senescence.

NMR relaxometry has been used in several studies to investigate plant cell structure and functioning (Hills and Duce, 1990; Van As, 1992). The ^{1}H-NMR signal originates almost entirely from water protons because other ^{1}H nuclei in the plant produce much less intense signals, as they correspond to molecules that are at a much lower concentration than water. The technique allows the measurement of longitudinal (T1) and transverse (T2) relaxation times and proton spin density. Water proton relaxation times are related to the rotational and translational mobility of water molecules (Van As, 2007). They are also modified by the mobility and structure of the surrounding macromolecules (i.e. starch, proteins, and polysaccharides) through proton exchange (chemical exchange). In plant cells, the water in different cell compartments has different chemical and physical properties and, therefore, different bulk T2 values. Moreover, relaxation times are affected by the exchange of molecules between different compartments that is determined by water diffusion and, therefore, by the compartment size and membrane permeability (Van der Weerd et al., 2002). The slow diffusion process between compartments results in multiexponential behavior of the relaxation signal. The multiexponential relaxation reflects water in cell compartments and, therefore, can be used to study changes in water distribution and properties at a subcellular level and, hence, can be used for the estimation of structural and volume transformations in cell compartments. The T2 relaxation time is more sensitive to small variations in water content and chemical exchange processes than T1 and, therefore, is usually preferred. Indeed, differences in T1 for the different compartments are relatively small, resulting in an averaging effect that results in poor discrimination between water compartments (Van As, 2007).

To date, NMR relaxometry has mainly been used for the characterization of fruit and vegetable tissues and has been shown to be effective in providing valuable information about cell organization (Sibgatullin et al., 2007). However, although a number of studies have contributed to the interpretation of the NMR results (Snaar and Van As, 1992; Hills and Nott, 1999; Marigheto et al., 2009), this is still not always straightforward, as the NMR signal depends both on the nature of the plant tissue and on the NMR measurement protocol. The situation is even more complex in the case of leaves, because leaves contain different tissue types characterized by different cell sizes and structures (Teixeira et al., 2005), and only a few studies involving NMR relaxometry in leaves have been reported. Changes in T2 in response to high temperature were investigated in wheat (*Triticum aestivum*; Maheswari et al., 1999) in order to develop a method for the detection of heat injury. McCain (1995) measured the T2 relaxation time of chloroplast and nonchloroplast water in maple (*Acer platanoides*) leaves by separating corresponding peaks in an NMR spectrum without taking into account the compartmentalization of nonchloroplast water. Oshita et al. (2006) investigated cell membrane permeability to water in spinach (*Spinacia oleracea*) leaves by measuring the T1 relaxation time of the leaf protoplasts without consideration of the subcellular structure. Qiao et al. (2005) attempted to associate NMR signal components with different chive (*Allium schoenoprasum*) cells using combined transverse relaxation and restricted diffusion measurements. Finally, Capitani et al. (2009) recently used a portable unilateral NMR instrument to detect the water status of leaves of herbaceous crops, mesophyllous trees, and natural Mediterranean vegetation under field conditions. Further investigations are necessary to improve leaf characterization by NMR, especially in the attribution of NMR signal components to the tissue and subcellular compartments. Progress in this field would make it possible to use the full potential of noninvasive NMR relaxometry in plant research and phenotyping.

Using NMR relaxometry, we describe here the differences in water status that occurred at tissue and cellular levels through different leaf ranks of well-irrigated oilseed rape plants, from the young leaves at the top of the canopy to the senescing older leaves at the bottom of the plant. The aim of the study was to show that changes that occur in the leaves while senescing can be related to changes in water distribution and cell structure. As these changes are directly linked to the modifications in cell compartment organization, especially

those occurring in the chloroplast, vacuole, and cell wall due to macromolecule degradation and N and carbon reallocation processes, this study was designed to contribute to the understanding of these physiological processes.

RESULTS

Changes in Physiological Traits during Leaf Development

The whole group of plants grown under homogenous conditions in a growth cabinet displayed a similar developmental pattern in terms of phenological and physiological status. The different leaf stages (corresponding to leaves of different ages) were collected from 8-week-old plants rank by rank and analyzed for physiological status (Fig. 1). All the individual plants used for measurement had a set of well-developed leaves, from the youngest green leaves at the top (leaf rank 8) to the yellowish and most senescent leaves at the bottom (leaf ranks 1 and 2). Chlorophyll content, stable from leaf ranks 8 to 6, decreased markedly from leaf rank 4 to 1 (Fig. 1A). The highest level of starch content was found at around leaf rank 6, again with a decrease in senescing leaves from ranks 4 to 1. Used as global indicators of leaf growth and development, this information ensures the choice of leaf ranks studied through NMR (i.e. rank 8 for younger fully expanded leaves, rank 6 for mature leaves, and ranks 4 to 1 for senescing leaves).

Figure 1B depicts dry and fresh weights of leaves, and Figure 1C shows the corresponding water content and water weight data. Dry weight (expressed per m^2 of leaf area) decreased from leaf rank 6 to leaf rank 1, whereas a considerable increase in fresh weight and water content was observed from leaf ranks 6 to 1. The senescence process was clearly associated with hydration (increase in the quantity of water per unit of leaf area) in leaf tissues, whereas dry matter was depleted. This phenomenon was also confirmed in the leaf water status experiment (Fig. 2), in which the increase in water content from the youngest (leaf rank 8) to the oldest (leaf rank 1) leaves was less pronounced but statistically significant. The ANOVA test showed also that differences in leaf water potential and osmotic potential of the youngest (leaf rank 8) and oldest (leaf rank 1) tissues, associated with an increase in fresh weight, were statistically significant. Turgor pressure, relative water content (RWC), and water deficit did not change significantly with senescence.

Chlorophyll a/b Binding Protein (Cab)/Senescence-Associated Genes (Sag): Molecular Milestones of Leaf Development

The physiological characteristics (chlorophyll content, starch deposition, and water status) provided a general pattern of leaf development along the plant axis. However, the physiological status of the individual plants studied varied to some extent in terms of

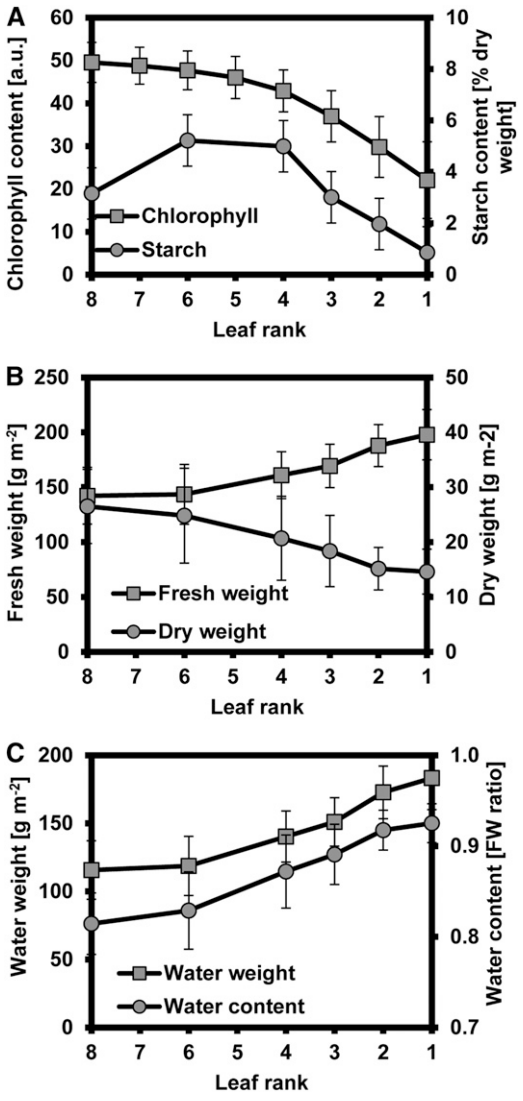

Figure 1. Changes in chlorophyll (in arbitrary units [a.u.]) and starch contents (A), fresh and dry weight per leaf area (B), and water weight per leaf area and water content in fresh weight (FW) ratio (C) in oilseed rape leaves during senescence. Values are means ± SD of 16 individual plants (P-1 to P-16).

leaf development due to growth conditions and heterogeneity of the microenvironment (see SD values in Fig. 1). In addition, these traits did not make it possible to detect slight physiological variations, as the senescence process occurred progressively from one leaf rank to another. In order to evaluate this variability between leaf ranks more precisely, the expression levels of genes previously used to describe the leaf development status of oilseed rape were followed (Gombert et al., 2006). Thus, the expression pattern of genes known to be up-regulated (*SAG12-1* coding a Cys protease) or down-regulated (*Cab* coding a chlorophyll *a*/*b*-binding protein) during leaf senescence was established for five plants throughout the vegetative axes (Fig. 3A). The concomitant measurement of *SAG12* and *Cab* gene transcript levels provided

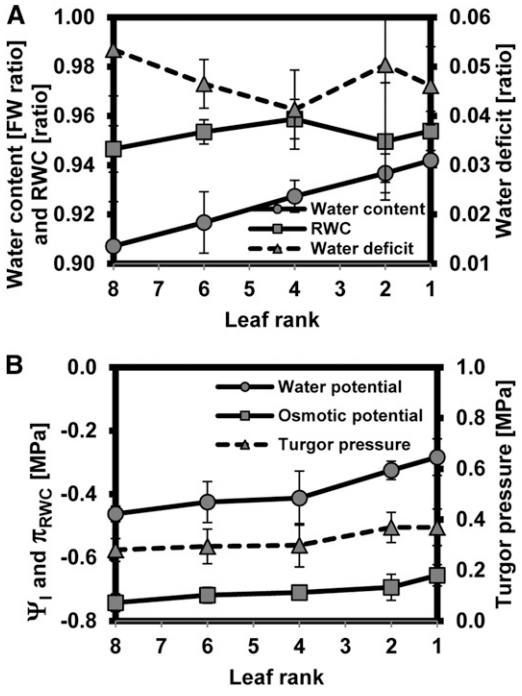

Figure 2. Changes in water content in fresh weight (FW) ratio, RWC, and water deficit (A) and leaf water potential (Ψ_l), leaf osmotic potential (π_{RWC}), and turgor pressure (B) in oilseed rape leaves during senescence. Values are means ± SD of four individual plants (P-17 to P-20).

accurate monitoring of the progression of leaf senescence and allowed a theoretical leaf rank to be seen as a critical transition step where the source status took precedence over the sink status (Fig. 3B). For instance, in the example shown, the expression of *Cab* and *SAG12* was relatively stable from leaf rank 8 to leaf rank 5, while from leaf rank 4, a strong decrease in *Cab* expression associated with an increase in *SAG12* was observed. The theoretical leaf rank differed from plant to plant and was identified in leaf ranks 1 to 4 (Table I). Therefore, it must be emphasized that, although the plants studied further by NMR displayed homogenous macroscopic phenological traits, individual differences were observed in terms of the physiological status of leaves of the same ranks. The *SAG12/Cab* value can be used to target leaves at the same development status, although it does not make it possible to define this status. For example, leaf rank 1 of plant P-1 was comparable to leaf rank 2 of plant P-11 and to leaf rank 3 of plant P-13. In addition, *SAG12/Cab* results suggested that leaf rank 3 corresponded to a younger leaf in plant P-1 than in plant P-6.

NMR Signal Evolution during Leaf Senescence

The relaxation decay in leaf samples corresponding to the separate CPMG (for Carr Purcell Meiboom Gill) data were described by three or four relaxation components depending on the developmental stage of the leaf. A typical example of the distribution of transverse relaxation times obtained by the maximum entropy method (MEM) for different development stages is given in Figure 4, with the peaks centered at the most probable T2 values and the peak areas representing the intensity of the T2 components. Three components were observed by the MEM method for the youngest leaf analyzed (Fig. 4A), with the shortest T2 component centered at about 3 ms and representing about 8% of the total signal intensity, the intermediate component centered at about 25 ms (19% of the signal intensity), and the longest T2 component centered at about 100 ms (73% of the signal intensity). For the example shown, the shortest component remained in the same range of T2 throughout leaf tissue aging, until the late senescence stage (leaf rank 1) when it disappeared. The T2 of the intermediate component was about 20 ms for all measurements, while its relative signal intensity decreased (from 19% to 13%, for leaf ranks 8 and 1, respectively). The T2 of the longest T2 component increased from the youngest to the most senescent leaf, starting progressively to split into two components between leaf ranks 3 and 2. Figure 4E shows four distinct components measured at leaf rank 2, with the two longest T2 components centered at about 190 and 340 ms, respectively. Finally, the T2 values of the two longest T2 components were about 220 and 450 ms for the late senescence leaf (Fig. 4F). The sum of relative signal intensities of the two longest T2 components increased from 73% to 87% with senescence (for leaf ranks 8 and 1, respectively).

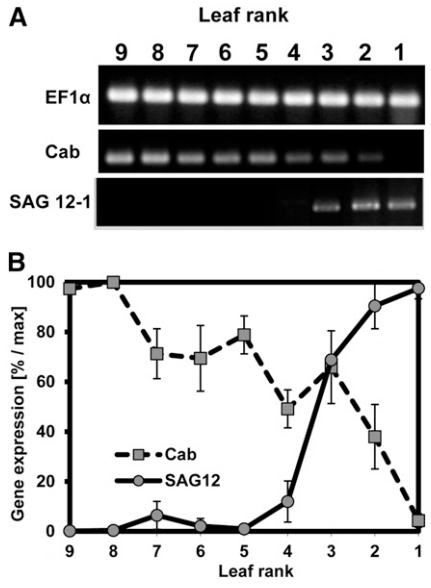

Figure 3. Characterization of leaf status in terms of the expression of *SAG12* and *Cab* (data from P-13) in oilseed rape leaves during senescence. A, RT-PCR of *SAG12-1* and *Cab* gene expression. *EF1α* was used as a complementary DNA synthesis and amplification control. B, Determination of the theoretical sink-source transition. Cab and SAG12-1 RNA are expressed in percentages related to the maximum (leaf 8 for Cab and leaf 1 for SAG12-1).

Table I. *Parameters of leaf water status and senescence and comparison of leaf ranks of different plants of oilseed rape*

The five plants for which critical transition of the *SAG12-Cab* ratio occurred are listed in the second column. Classification of the plants (P-1 to P-16) for which the longest T2 component split into two components is given in the third column.

Leaf Rank	Plants for Which Critical Transition of *SAG12-Cab* Ratio Occurred	Plants for Which Splitting of the Longest T2 Component Occurred
1	P-1	P-1, P-2, P-3
2	P-11, P-12	P-5, P-7, P-8, P-11, P-12, P-14
3	P-13	P-10, P-13, P-16
≥4	P-6	P-6, P-9, P-4, P-15

The T2 distribution shown in Figure 4 was very similar for the 16 plants analyzed (data not shown). However, some differences were observed between plants with regard to the leaf rank where the split occurred, confirming previously suspected physiological heterogeneity within leaf ranks. In Table I, the plants are classified according to the leaf rank at which the longest T2 component split into two components. It can be seen that the critical transition of the *SAG12/Cab* ratio (second column) fitted well with the NMR results for the five plants studied.

The discrete solutions for the complete decay curve (free induction decay [FID] + CPMG) obtained by the Levenberg-Marquardt algorithm agreed to a great extent with the MEM results of the separate CPMG curve and in addition provided access to the first component, relaxing at about a few tens of microseconds (Table II). The relative intensity of this component, $I_{0(comp.1)}$, decreased during senescence, while its $T_{2(comp.1)}$ seemed to increase only for the most senescent leaf.

As previously explained, the NMR signal from vegetable tissue can be attributed mainly to protons from water molecules, characterized by T2 relaxation times in the range of a few milliseconds or more. However, T2 components relaxing at lower relaxation times (in the range of 10–100 μs) in principle correspond to solid matter. In order to check this assumption, the intensity of the first component of the FID-CPMG signal at

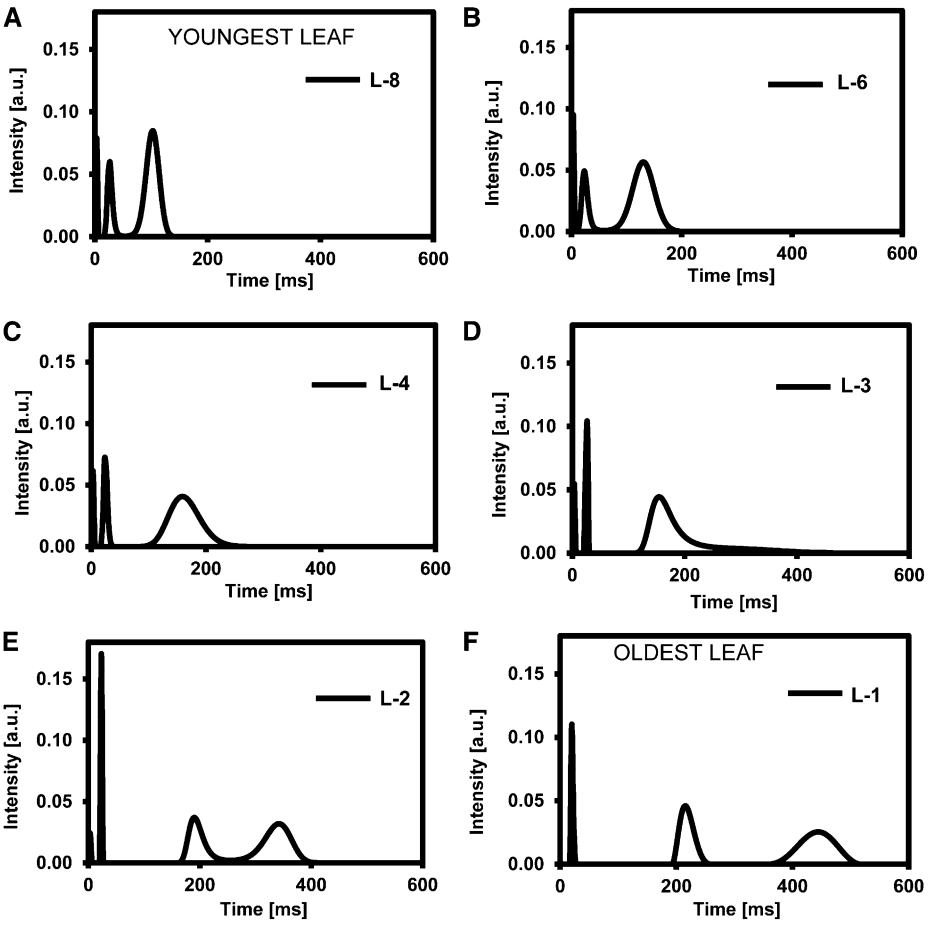

Figure 4. Transverse relaxation time distribution (MEM) calculated from the CPMG signal for oilseed rape leaves of six different leaf ranks (L). Data shown correspond to P-5.

equilibrium state [$I_{0(comp.1)}$] was correlated with dry matter mass and the sum of the intensities of the other components [$I_{0(comp.2-5)}$] to the water mass. Both relationships (Fig. 5) were linear and positive [r^2 = 0.75 for $I_{0(comp.1)}$ and r^2 = 0.89 for $I_{0(comp.2-5)}$] and demonstrated that the signal from the first component of the FID-CPMG sequence corresponded to the dry matter and the sum of the signals from the other components corresponded to the water, independent of leaf age. In addition, as already explained, the results confirmed that the water and dry matter masses depended on leaf age. The dry matter mass of leaf samples (dry weight per leaf area) and $I_{0(comp.1)}$ for young leaves were relatively high and decreased for mature and senescing leaves, while the water mass and $I_{0(comp.2-5)}$ were highest in the most senescent leaves (ranks 1 and 2; Fig. 5).

Figure 6 shows the relative signal intensities and mean values of T2 for the 16 plants studied, expressed in leaf water weight (LWW) for all components, obtained by the Levenberg-Marquardt algorithm. Since the total intensity of components 2 to 5 [$I_{0(comp.2-5)}$] was strongly correlated with total water mass for young to senescent leaves for all plants (Fig. 5B), variations in water mass related to each component were calculated through leaf development (Fig. 6A). The results showed that the increase in LWW (expressed in water mass per leaf area) of senescing leaves was due to the increase in the amount of water associated with components 4 and, particularly, 5. However, LWW associated with component 3 decreased slightly (Fig. 6A), while that of component 2 remained unchanged. Note that the LWW increase reflected cumulative effects of both increases in signal intensity and water mass.

The overall trend for T2 of components was the same as in the example given in Table II. The T2 of components 4 and 5 increased markedly (Fig. 6C), which could be related to the increase in the amount of water associated with these components (Fig. 6A).

Correlation between NMR Signal and Physiological Traits of Leaves

Principal component analysis (PCA) was performed in order to draw up a general framework of all the variables measured. The first principal component (PC1; 72.8% of total variance) appeared to be mainly assigned with leaf development (Fig. 7A). First, young leaves (leaf rank 6) were characterized by high levels of chlorophyll and starch content and dry matter (right part of PCA; Fig. 7B), whereas the most senescent leaves (leaf ranks 1 and 2) were characterized by higher water content (left part of PCA; Fig. 7B). This is in agreement with the phenomenon of dry weight lost during senescence, associated with chlorophyll and starch breakdown. Moreover, the results demonstrated that this loss of dry weight was correlated with an increase in leaf water content and, therefore, the hydration of leaf tissues. Second, the high intensities of the second [$I_{0(comp.2)}$] and third [$I_{0(comp.3)}$] components of the NMR signal were associated with the youngest leaves (right part of PCA; Fig. 7B), whereas the high total intensity of components 4 and 5 [$I_{0(comp.4-5)}$] and the high value of the corresponding $T_{2(comp.4-5)}$ were associated with the most senescent leaves (left part of PCA; Fig. 7B).

The Pearson correlation coefficients of the PCA set out in Figure 7 are shown in Table III.

Relationship between NMR Signal and Cell Structure

Optical micrographs from young and senescent leaf tissues are shown in Figure 8. Four parallel layers of cells can be observed on the images (upper and lower epidermis, palisade and spongy layers). As expected, the palisade layer was composed of elongated, relatively tightly packed cells arranged in two to three rows, while the spongy layer was made up of rounded cells with large intercellular spaces. Moreover, most of the chloroplasts were stuck to the plasmalemma, especially in the palisade mesophyll. The upper and lower monolayered epidermal cells can be easily seen in the images. Both the length and width of the palisade mesophyll cells increased considerably in senescing tissues, whereas those of the spongy mesophyll cells seemed to remain almost unchanged. The number of chloroplasts per cell appeared to remain stable throughout the senescence process; consequently, their relative volume decreased compared with the relative volume of the vacuole. The regular shape of the chloroplasts was preserved in most of the senescent leaves studied (Fig. 8, C and D), indicating that the end of the senescence

Table II. *T2 and corresponding relative intensities for the complete decay curves (FID + CPMG) obtained by the Levenberg-Marquardt algorithm for six oilseed rape leaves presented in Figure 4 (P-5)*

Leaf Rank	Component 1		Component 2		Component 3		Component 4		Component 5	
	I_0	T2	I_0	T2	I_0	T2	I_0	T2	I_0	T2
	%	ms	%	ms	%	ms	%	ms	%	ms
8	5	0.03	9	2	19	27	66	103	–	–
6	6	0.03	10	3	18	27	66	132	–	–
4	4	0.03	7	2	18	27	71	166	–	–
3	3	0.03	7	3	18	36	72	195	–	–
2	3	0.03	4	1	14	23	32	196	47	341
1	3	0.07	–	–	12	21	36	222	48	448

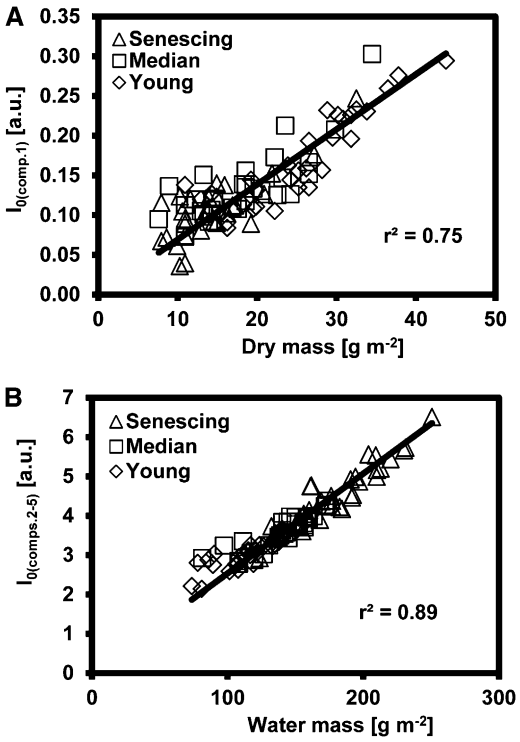

Figure 5. Correlations between the intensity (expressed in arbitrary units) of the first components of the FID-CPMG signal assumed to correspond to the solid proton fraction [$I_{0(comp.1)}$] and dry matter mass per leaf area (A) and between the sum of the intensity of other components of the FID-CPMG signal assumed to correspond to the water proton fraction [$I_{0(comps.2-5}$] and water mass per leaf area (B) for young (ranks 6 and 8), median (ranks 3–5), and senescing (ranks 1 and 2) oilseed rape leaves. Signal intensity was corrected for the receiver gain. Values correspond to 16 individual plants (P-1 to P-16).

process had not been reached, even for these leaves. Finally, the area of palisade cells of senescent leaves was estimated to be about four times greater than that of the corresponding young leaf tissues.

Variations in the volume of vacuoles, chloroplasts, and cell wall (Fig. 9A) were estimated (see "Materials and Methods," Eqs. 7–9). A considerable decrease in the relative volume of the plastidial compartment was observed as senescence progressed. In the young leaves, the chloroplast volume was roughly estimated to be about 40% of the cell volume, and it dropped to below 20% in the most senescent leaves. In contrast, the size of the vacuole increased from about 55% to almost 80%. Finally, our method did not permit the clear detection of variations in cell wall volume, although the results seemed to indicate a minor volume reduction (Fig. 9A).

Figure 9B depicts the relative intensities of the NMR signal components for young and senescent leaves that can be considered as an estimation of water distribution in cell compartments. Similar patterns can be observed in the NMR and microscopy results on comparing Figure 9, A and B. For young leaves, the vacuole occupied about 55% of the cell volume, whereas the intensity of components 4 + 5 was about 65%. The relative vacuole volume for senescing leaves increased to about 80%, and a similar phenomenon was observed for the relative intensity of components 4 + 5 (approximately 85%). On the other hand, chloroplast volume in young leaves was estimated to be about 40%, decreasing to about 20% in senescing leaves, whereas the relative intensity of the third component decreased from about 20% to about 10%. Finally, cell wall volume was estimated to be about

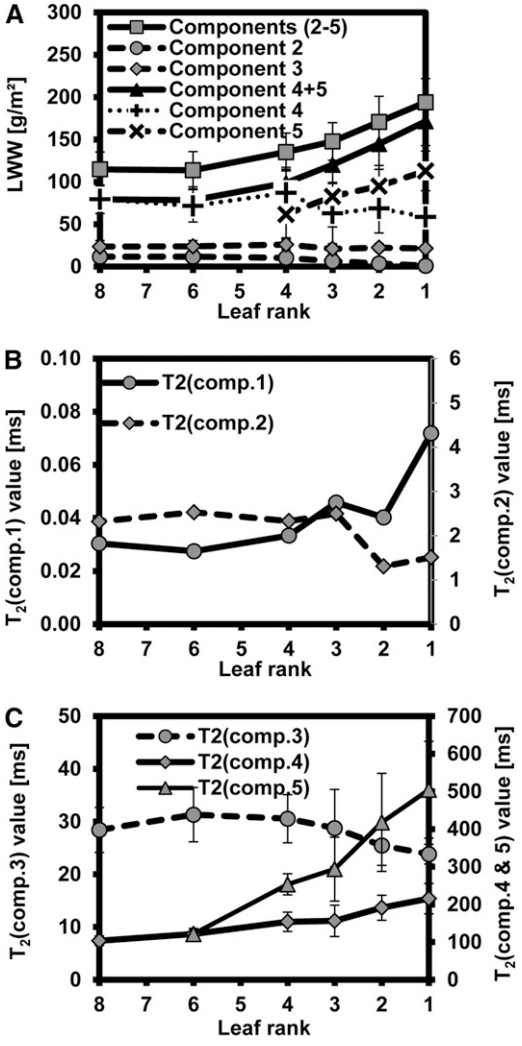

Figure 6. NMR relaxation parameters of oilseed rape leaves during senescence according to leaf rank. T2 and corresponding I_0 values for the complete decay curves (FID + CPMG) were obtained by the Levenberg-Marquardt algorithm. A, Water distribution in the water-associated components (2–5) expressed as $LWW_i = \frac{I_{0i}\ x\ m_w}{A}$, where LWW_i is the specific LWW of the i^{th} signal component expressed in g m^{-2}, with m_w as water mass per leaf sample used for NMR analysis (in g), A as leaf sample area (in m^2), and I_{0i} as relative intensity of the i^{th} signal component (as a ratio of the total signal of water-associated components 2–5). B and C, Transverse relaxation times. Values correspond to 16 individual plants (P-1 to P-16).

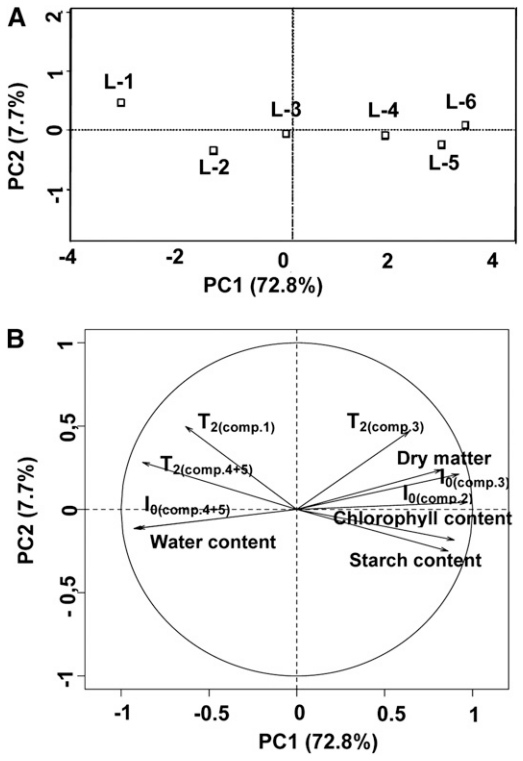

Figure 7. PCA of 10 multivariate data [chlorophyll, starch, and water contents, dry matter, $T_{2(comp.1)}$, $T_{2(comp.3)}$, and $T_{2(comp.4+5)}$, and $I_{0(comp.2)}$, $I_{0(comp.3)}$, and $I_{0(comp.\ 4+5)}$] corrected for the receiver gain and the sample weight of the six leaves of six different leaf ranks (6–1) from 11 oilseed rape plants grown in standard conditions. A, Score (L = leaf rank) plots for PC1 and PC2. B, Loading plot on the factorial plane made of the first two principal components (PC1 and PC2). PC1 and PC2 axes explain 80.5% of the total variance. Dots are means of up to 11 independent biological replicates.

5% and 3% for young and senescing leaves, respectively, and the relative NMR signal intensity of the second component decreased from 9% to 2% according to leaf maturity.

It should be noted that the variations in the volumes of vacuoles, chloroplasts, and cell wall were estimated roughly, as the spongy layer and the upper and lower epidermal cells occupying the leaf surface were ignored in the analysis. Additionally, the exchange of protons between different cell compartments over the biological membranes can affect the relative intensities of different NMR signal components.

DISCUSSION

Senescence Induced Changes at the Cell Level

The biochemical markers for the identification of leaf senescence used in this study have already been described in the literature (Masclaux et al., 2000; Desclos et al., 2008). The decreases in chlorophyll and starch content (Fig. 1) that we observed in senescent leaves were in accordance with the literature (Diaz et al., 2005; Albert et al., 2012). However, although these biochemical traits are relevant to providing a general view of senescence across plant shoots (Gombert et al., 2006), they are not precise enough to be used for comparisons between leaf ranks from different plants. Molecular markers such as *SAG12/Cab* gene expression (Gombert et al., 2006) provided a more precise description of changes in leaf development (Fig. 3), although handling them is fairly complex.

The senescence process has been well described in several reviews (Thomas and Stoddart, 1980; Buchanan-Wollaston et al., 2003; Lim et al., 2007), and as far as we are aware, it is commonly accepted that water loss occurs in leaves during senescence (McIntyre, 1987). The decrease in specific leaf dry weight during senescence, reflecting the drain of organic constituents from the leaves to other plant organs, has also been described (McIntyre, 1987; Malagoli et al., 2005; Fischer, 2007). In this study, as expected, a decrease in dry weight was observed for senescing leaves (Fig. 1B). However, an increase in water content was observed (Fig. 1C), leading to an increase in total specific LWW. Moreover, a relatively high increase in cell size associated with tissue hydration of leaves during natural senescence was observed (Figs. 8 and 9). This increase in cell size has not, to our knowledge, been previously reported in the literature. Thomas and Stoddart (1980) described senescing leaves with increasingly vacuolated cells and

Table III. *Pearson correlation coefficients of the data presented in Figure 7*

CC, Chlorophyll content; DM, dry matter; SC, starch content; WC, water content.

	CC	DM	$I_{0(comp.2)}$	$I_{0(comp.2)}$	$I_{0(comp.4+5)}$	SC	$T_{2(comp.1)}$	$T_{2(comp.3)}$	$T_{2(comp.4+5)}$	WC
CC	1.00									
DM	0.59	1.00								
$I_{0(comp.2)}$	0.82	0.85	1.00							
$I_{0(comp.3)}$	0.82	0.75	0.89	1.00						
$I_{0(comp.4+5)}$	−0.81	−0.75	−0.85	−0.86	1.00					
SC	0.85	0.61	0.82	0.72	−0.71	1.00				
$T_{2(comp.1)}$	−0.50	−0.45	−0.64	−0.48	0.47	−0.53	1.00			
$T_{2(comp.3)}$	0.49	0.44	0.62	0.68	−0.55	0.46	−0.33	1.00		
$T_{2(comp.4+5)}$	−0.89	−0.57	−0.80	−0.74	0.78	−0.83	0.58	−0.48	1.00	
WC	−0.76	−0.93	−0.92	−0.85	0.83	−0.74	0.52	−0.50	0.75	1.00

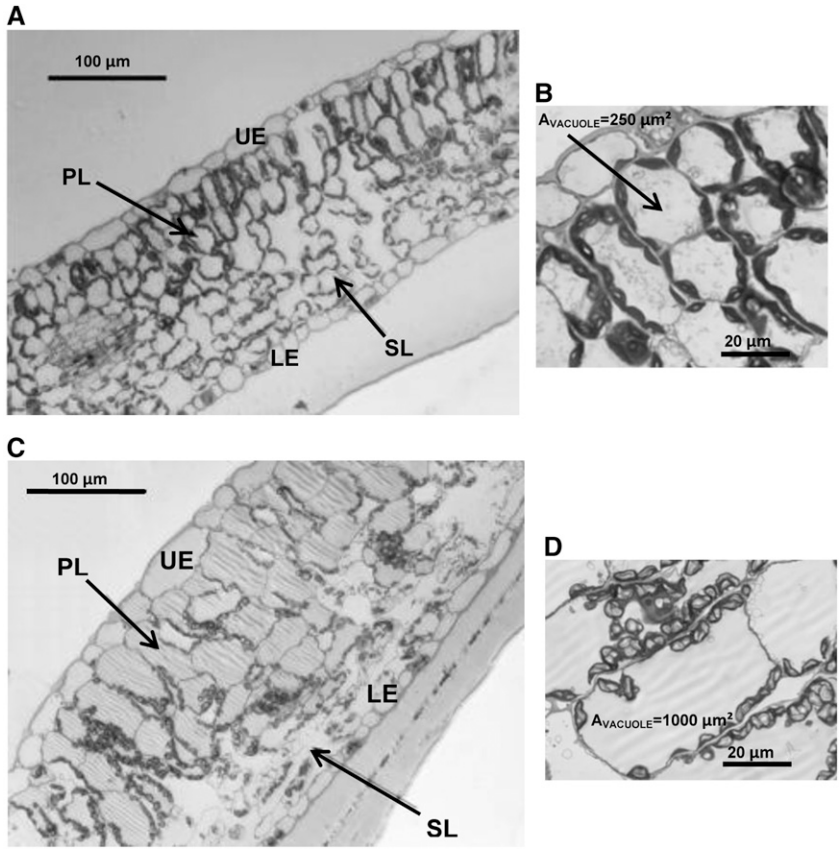

Figure 8. A, Light micrograph of young oilseed rape leaf tissues. B, Enlargement of the palisade cells in A. C, Light micrograph of senescent oilseed rape leaf tissues. D, Enlargement of the palisade cells in C. LE, Lower epidermis; PL, palisade layer; SL, spongy layer; UE, upper epidermis.

with a diminishing rim of cytoplasm, but they did not report cell enlargement. Keech et al. (2007) reported an increase in the perimeter of mesophyll cells of Arabidopsis leaves during senescence induced by dark treatment. The cell enlargement process has been reviewed by Cosgrove (1993, 1999). It occurs prior to cell growth associated with dry matter production and depends on the ability of the wall to loosen and to undergo stress relaxation. Cell wall extensibility is mediated by several protein factors, especially α-expansin expression (Cosgrove, 1999). The consequence of the cell enlargement process is water uptake. This process has not previously been reported in senescing tissues, although α-expansin expression has been studied during floral development. It has been linked to an early development stage corresponding to the rapid expansion associated with cell growth but was also found in senescing floral tissues (Gookin et al., 2003). Finally, Reid and Chen (2007) reported that cell wall loosening also occurred in senescing flower tissues due to the degradation of cell wall macromolecules.

The results of our study, micrographs (Fig. 8) and measurements of water status (Fig. 2), clearly demonstrated that a process of cell enlargement occurred in senescing leaves (especially for palisade cells) and that it was associated with cell hydration. Considering the trend in cell wall volume estimated from the leaf tissue micrographs (Fig. 9) and the observations reported for flower tissues (Reid and Chen, 2007), this process could be explained by the degradation of cell wall macromolecules that induces changes in the fibrillar structure of the cell wall and, consequently, causes water uptake from adjacent tissues. In our study, the slight and consistent increase in water content was associated with a slight increase in leaf water potential and osmotic potential (Fig. 2), probably reflecting tissue hydration. We demonstrated that this variation in leaf water content was not linked to a water stress event, as the water deficit remained constant. As the RWC (see "Materials and Methods," Eq. 4), which can be expressed as RWC = water content/(turgid weight/fresh weight − dry weight/fresh weight), remained unchanged, water content increase and dry weight decrease, associated with the fresh weight at full turgor increase, suggested an increase in cell wall elasticity. The latter is in agreement with the micrograph observations.

Interpretation of the NMR Signal of Senescing Leaves

The results of previous NMR studies performed on leaves differ from our results, as the NMR signal depends on leaf tissue type and on the measurement and signal-processing protocols. For instance, T2 measurements in wheat leaves (Maheswari et al., 1999) were performed by the CPMG method at the same magnetic field as that used in our study (20 MHz) but with considerably fewer sampling points (250 instead

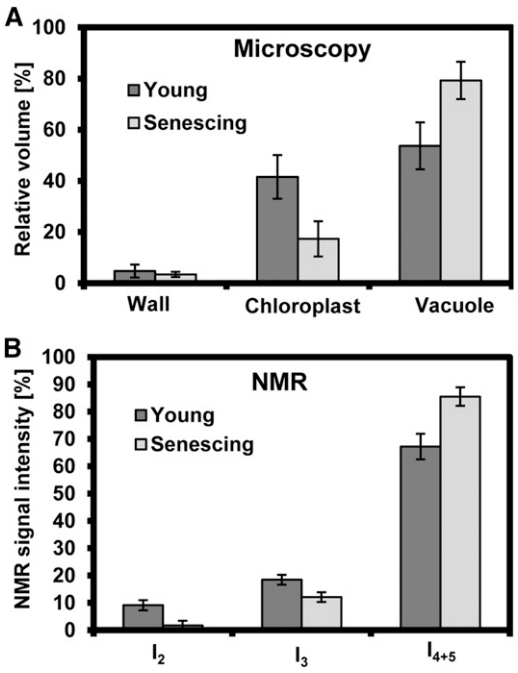

Figure 9. Relative volumes of the cell wall, chloroplast, and vacuole of young (ranks 6 and 8) and senescing (ranks 1 and 2) oilseed rape leaves estimated from the light and electron micrographs (A) compared with the relative NMR signal intensities of liquid components 2, 3, and 4 + 5 (B) in %. Eighteen leaves of five plants were used for microscopy studies.

of 6,000) and with longer pulse separation (0.5 ms instead of 0.1 ms used in our study) at temperatures from 35°C to 58°C. They obtained biexponential T2 decay, with the longer T2 component of T2 = 130 to 180 ms and I_0 = 65% to 70% attributed to intracellular water and the shorter component of T2 = 40 to 60 ms attributed to extracellular and hydration water. These two components correspond roughly to the two longest T2 components measured in our study in relatively young oilseed rape leaves (Table II). The T2 component relaxing at 3 ms in oilseed rape leaves was not observed because of the relatively long pulse space and the very small number of points sampled for the CPMG curve. Finally, in the study of Maheswari et al. (1999), the CPMG decay curve was acquired over 250 ms, which was not long enough for reliable fitting of the curve, since the baseline was not reached (last point $< 1.4 \times T_{2\text{-max}}$). On the other hand, Capitani et al. (2009) investigated the leaves of several species using a portable unilateral NMR apparatus (18.153 MHz) characterized by an inhomogenous magnetic field that did not allow measurement of the FID signal and produced shortening of the T2 values measured. Relaxation decays in the unstressed leaves were described by two or three exponential decays with T2 values of up to 40 ms. This approach has been demonstrated to be promising for application in field conditions, but it was not focused on interpretation of the NMR signal. Any comparison with our results thus seems difficult. The results of studies on chive tissues (Qiao et al., 2005) performed at 300 MHz were interpreted at the tissue level; T2/diffusion peaks were assigned to cells of different tissue types, such as palisade and spongy layers and xylem vessels. The subcellular level was not considered in that study, although in green leaf tissues, chloroplasts represent a significant level of cell volume. For instance, in wheat, chloroplasts occupy up to 70% of the surface area of mesophyll cells and approximately 20% of their volume (Ellis and Leech, 1985). In addition, they are believed to have distinct relaxation and diffusion properties (Van As, 2007) due to their small size (about 6 μm in diameter). The results of T2 measurements obtained in maple leaves at 300 MHz using a different approach (McCain, 1995) differed considerably from those in chive tissue. Chloroplast water was discriminated, and its T2 was surprisingly estimated to be higher than the T2 of non-chloroplast water.

Except for the last study mentioned, the longest T2 component is generally associated with vacuolar water (Van As, 2007), because of its relatively high mobility. It usually also has the highest relative intensity, as the vacuole encloses the highest amount of cell water (Teixeira et al., 2005). As explained above, young and mature leaves (leaf ranks 8–3) were characterized in our study by three water-associated components (Fig. 4). According to the literature, the highest T2 component could be attributed to the vacuole, as it represented about 70% of the total water and had a relatively long T2 (about 100–200 ms) depending on the leaf rank (Table II). In senescing leaves, this water fraction was distributed between two NMR components, still representing three-quarters of the total water. This could be explained by tissue heterogeneity that was emphasized during senescence. In fact, differentiation in cell morphology between palisade and spongy layers was observed on light micrographs (Fig. 8) and showed that cell enlargement occurred only for palisade cells. This heterogeneity of cell size may affect the NMR relaxation times (Van der Weerd et al., 2002) of the two cell types (Qiao et al., 2005), resulting in the increase in T2 of enlarged palisade cells. Finally, the relative signal intensity of the two longest T2 components and its trend during senescence approximately matched the relative volume of the vacuole estimated from the light micrographs (Fig. 9).

T2 values of these vacuole-associated components increased during senescence, particularly the T2 of the fifth component (Fig. 6). This can be explained by the increase in vacuole size, according to the sensitivity of T2 to compartment size (Van der Weerd et al., 2002), and by water influx induced by senescence. On the other hand, the entry of dead-end metabolites of organic component degradation occurring during the senescence process (Buchanan-Wollaston et al., 2003; Wada et al., 2009) could shorten T2 values through chemical exchange between protons of these metabolites and water protons. However, the latter process seemed to be minor compared with the effects of water

content increase due to the rise in water amount in the vacuolar compartment.

The overall results of this study indicated that the third T2 component could probably be assigned to the plastidial water. Chloroplast volume and its trend during senescence estimated from the micrographs matched well the relative intensity of the third T2 component (Fig. 9). The covering of the mature cell surface by chloroplasts varies considerably in higher plants, with a total chloroplast area per unit of plan area of the cell greater than 70% in spinach and as low as 25% in *Nicotiana glutinosa* (Honda et al., 1971). However, as shown by Ellis and Leech (1985), the chloroplast volume is fairly constant in leaf mesophyll tissue for any given species. Their results demonstrated that chloroplasts represented up to 40% of total cell volume for mature leaves. As the chloroplast dimensions measured (about 6 μm diameter and 2 μm thick) were in agreement with the literature (Ellis and Leech, 1985), their volume can be estimated to be about 50 μm^3, also in accordance with the literature (Zellnig et al., 2010). On the other hand, plastids are distributed as a peripheral monolayer in mesophyll cells (Ellis and Leech, 1985) in the same way as in cells of equivalent size and shape. Their average number, therefore, may be estimated as about 90 chloroplasts per cell (with an estimated volume of less than 12,000 μm^3) and the relative volume to be about 40%. However, this percentage may be slightly overestimated, as in species such as wheat there are fewer than 70 chloroplast for cells as large as 1,400 μm^2 (Ellis and Leech, 1985). Following the hypothesis that chloroplast water content is about 50%, based on the ratio of the relative volumes of well-watered stroma and lipid-enriched thylakoids and plastoglobules (Zellnig et al., 2010) and as the water content increases markedly in the gerontoplast due to the loss of thylakoid membranes, the estimated volume of plastidial water weighed by water content fitted even better the amount of water computed from the NMR signal intensity. The T2 of the third component has only been reported for maple leaves (McCain, 1995) to our knowledge. Its value in that study was surprisingly high (about 40 ms), considering that measurements were performed at a relatively high magnetic field (300 MHz). The plastid T2 obtained here (Table II) was in the same range, although it was measured at 20 MHz. However, in view of the differences in size between plastidial and vacuolar compartments, such plastidial T2 values appeared to be in agreement with the T2 found for vacuoles.

Finally, the low T2 value (Table II) of the second component (about 3 ms) should correspond to that of water close to macromolecules or to solid surfaces (Van As, 2007), and this component represented about 10% of the cell water (Table II). Therefore, different hypotheses can be proposed for its attribution, such as starch hydration water or cell wall water. First, the T2 value measured (Mariette et al., 1999; Tang et al., 2000) and the fact that component 2 disappeared in the most senescent leaves at the same time as the starch suggest that it may correspond to water in starch granules. However, according to Mariette et al. (1999), the mass of water enclosed in starch granules per total starch mass is 0.3829 g g^{-1}, and it was estimated to be 0.3% for leaf rank 6. This is far beyond the relative intensity of component 2. On the other hand, the T2 values measured (Table II) may indicate that component 2 corresponds to the water in rapid exchange with cell wall protons according to the attribution proposed for fruit (Sibgatullin et al., 2007). Additionally, the relative water volume enclosed in the cell wall could correspond to the relative NMR signal intensity of component 2 (Fig. 9). The fact that the second component disappeared in the most senescent leaves could be explained by cell wall thinning associated with macromolecule degradation.

As demonstrated above, the first component was attributed to dry matter protons. The analysis performed did not allow going into further details. Indeed, the sole organic compound quantified was starch, and it represented between 1% and 5% of the dry weight, while dry matter content represented between 20% and 8% of the total weight, depending on the leaf senescence stage. On the other hand, the intensity of the first component relaxing at about 30 μs was about 5% of the total FID-CPMG signal.

The PCA analysis (Fig. 7) showed that chlorophyll breakdown and starch degradation were associated with leaf aging. The NMR signal was shown to be able to describe this senescence-induced subcellular water redistribution. For instance, the relative intensity of

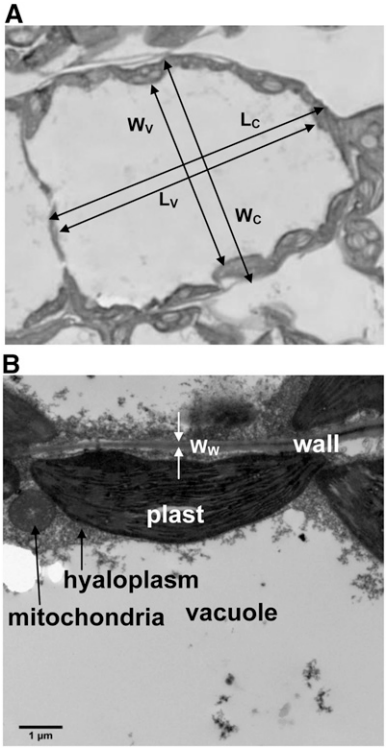

Figure 10. Light (A) and electron (B) micrographs of an oilseed rape leaf cell. L_C, Cell length; L_V, vacuole length; W_C, cell width; W_V, vacuole width; W_W, wall thickness.

components 4 and 5 [$I_{0(comp.4+5)}$] and the transverse relaxation times [$T_{2(comp.4+5)}$] associated with vacuole water were positively correlated with senescence, describing water entry and vacuole enlargement. On the other hand, the relative intensity of the third component [$I_{0(comp.3)}$] was negatively correlated with senescence, describing the decrease in the relative volume of the chloroplasts.

CONCLUSION

This study demonstrates that NMR relaxometry is a powerful technique for monitoring leaf development, as T2 measurements provide access to the cell structure through subcellular water distribution. Applied to a wide leaf panel, this technique was shown to be able to detect slight variations in senescence evolution accurately. Combining NMR with microscopy and physiological characterization throughout the senescence process contributed to understanding of the attribution of NMR signal components. The results represent an important step toward further studies investigating the biological significance of the signal.

One of the main applications of leaf NMR relaxometry would be in field applications, such as leaf tagging and plant phenotyping. It will be necessary first to investigate the leaf NMR signal in relation to different environmental conditions, such as water or N depletion. As field applications require portable NMR devices, and this will inevitably weaken the quality of the signal, this aspect should be also evaluated.

One other important application of the proposed technique will be to improve our understanding of plant functioning at the cell and tissue levels. Changes in water distribution and cell structure during any physiological process or under abiotic or biotic stress are not directly accessible with currently used techniques; therefore, NMR represents a promising and powerful technique for plant investigations.

MATERIALS AND METHODS

Plant Material, Experimental Design, and Growth Conditions

About 100 seeds of oilseed rape (*Brassica napus* genotype Tenor) were individually weighed, and the 45 most homogenously sized seeds were selected. Each working day for 3 weeks, three seeds were sown in individual containers filled with a growing medium (FALIENOR 9226-6F2) containing 65% light peat, 20% dark peat, and 15% perlite. Three-week-old seedlings were individually planted into 2-L pots filled with the same growing medium and grown in a growth cabinet for 5 weeks. Plants were watered throughout the growing period with a fertilizing solution (Liquoplant bleu) used at 3‰, and irrigation was adjusted to the evaporation-transpiration rate of the pots. The growth cabinet conditions were 14 h of light (at 200 μmol photons m^{-2} s^{-1})/10 h of dark, relative humidity of 75%/90%, and temperature of 20°C/18°C.

Sixteen of the 45 plants (P-1 to P-16) were selected (about one out of every three plants analyzed) in order to obtain homogenous plants with a wide range of leaf development status, characterized by the nondestructive measurement of chlorophyll content.

Direct measurements of leaf water status were performed in an additional experiment on plants grown in the same conditions as described above. For these measurements, 10 seeds were sown, six 3-week-old seedlings were individually planted, and thereafter, four plants were selected (P-17 to P-20).

Sampling

For the 16 plants selected (P-1 to P-16), leaf tissues were collected from six leaves (four senescing leaves, one mature leaf, and one young leaf) for NMR measurements, and microscopy studies were performed on the same leaves as for NMR analysis but for only five plants (plants P-1, P-5, P-6, P-10, and P-11). Starch was quantified for all leaves from all 16 plants, and molecular analyses were performed for all leaves from five plants (plants P-1, P-6, P-11, P-12, and P-13).

Six leaf discs of 8 mm in diameter were cut from the limb tissue for the NMR experiment. In order to obtain homogenous tissues, discs were taken from each side of the central vein as close as possible to the vein by avoiding lateral nervures. Discs were then placed in NMR tubes, which were closed with a 2-cm-long Teflon cap to avoid water loss during measurements.

For microscopy studies, 18 leaves from five plants were analyzed. About 30 1-mm^2 leaf samples per leaf were taken with a small punch around the discs used for NMR analysis. The leaf samples were immediately fixed in a solution of 2.5% (m/v) glutaraldehyde and 2% (m/v) paraformaldehyde in 0.1 M phosphate buffer, pH 6.8.

For starch quantification and gene expression, two sets of 20 leaf discs (diameter of 8 mm) were collected from all leaves near the location where NMR and microscopy were performed, frozen in liquid N, and stored at 80°C.

For the direct measurement of leaf water status, five leaves (leaf ranks 1, 2, 4, 6, and 8) were selected from each plant (P-17 to P-20). Prior to leaf water status measurements, NMR measurements were performed on all selected leaves.

Starch Quantification

Starch was quantified according to the method proposed by Smith and Zeeman (2006). Starch was extracted from 30 mg dry weight of freeze-dried lamina leaf tissue using 1 mL of phosphate buffer (0.2 mol L^{-1}, pH 6.5) for 20 min at 95°C. The supernatant was collected after centrifugation at 14,000*g* for 5 min at 4°C. The extraction step was repeated twice, and the supernatants were pooled. Starch quantification was performed following the manufacturer's recommendations (Sigma; STA20) after hydrolysis by α-amylase and amyloglucosidase. Starch content was expressed in Glc equivalents after subtraction of free Glc content.

Cab/SAG Molecular Markers

RNA Extraction

Total RNA was extracted from 500 mg fresh weight of frozen lamina leaf tissue. The RNA isolation protocol based on phenol extraction and lithium chloride precipitation was applied as described by Verwoerd et al. (1989). The quantity and quality of RNA samples were assessed by spectrophotometry with a NanoDrop ND 1000.

Reverse Transcription-PCR Analysis

Total RNA (2 μg) treated with RNase-free DNase I (Fermentas, Thermo Fisher Scientific) was reverse transcribed with Moloney murine leukemia virus reverse transcriptase (Q-BIOgene; MP Biomedicals) following the manufacturer's recommendations. PCR was performed using specific primers for the oilseed rape *Cab* gene *LHCII type I* (AY288914; forward primer 5′-GGCAGCCCATGGTACGGATC-3′ and reverse primer 5′-CCTCCITCGCT-GAAGATCTGT-3′), primers shared by *SAG12-1* (AF089848; forward primer 5′-GTTTTGTTTAGCCAAAGTCAAACA-3′ and reverse primer 5′-CGGCGGA-AGATTGGCT-3′), and primers designed from Arabidopsis (*Arabidopsis thaliana*) *EF1α* (X16430; forward primer 5′-GTTTTGTTTAGCCAAAGTCAAACA-3′ and reverse primer 5′-CGGCGGAAGATTGGCT-3′). All the PCRs were performed with Q biogen Taq polymerase for 35 cycles for *EF1α*, 27, 29, and 31 cycles for *SAG12-1*, and 22, 24, and 26 cycles for *Cab*. After 5 min at 95°C, reverse transcription (RT)-PCR was performed by cycles including 15 s at 95°C, 40 s at 60°C, and 72°C for 1 min, followed by one cycle at 72°C for 10 min. Products of 183, 587, and 290 bp were amplified from *BnEF1α*, *BnSAG12-1*, and *BnCab* gene complementary DNAs, respectively, as verified by sequencing. RT-PCR products were separated by agarose gel electrophoresis. Each PCR product was quantified using ImageJ software and normalized using the intensity of the *EF1α* RNA signal. For

all RT-PCRs, *EF1α* RNA was used as a complementary DNA synthesis and amplification control. The relative expression of *Cab* and *SAG12-1* was determined with reference to the maximum and represented the mean of PCR products obtained after different PCRs with various numbers of cycles.

NMR Relaxometry

NMR relaxometry measurements were performed on a 20-MHz (0.47-T) spectrometer (Minispec PC-120; Bruker) equipped with a thermostatted probe. The temperature was set at 18°C. T2 was measured using the combined FID-CPMG sequence. The FID is known to be affected by the heterogeneity of the magnetic field B_0. The FID relaxation rate ($1/T_{2FID}$) can be described as the sum of the intrinsic relaxation rate ($1/T_{2intrinsic}$) and the relaxation related to B_0 inhomogeneities ($1/T_{2inhomogeneity}$). In the experimental condition used (0.47 T and very short sampling time; see below), the $T_{2inhomogeneity}$ was equal to 1.7 ms. Then for T2 less than 100 μs, its effect was negligible and the T2 measured from the FID was equal to $T_{2intrinsic}$. The CPMG sequence was used for measurements of T2 longer than 500 μs because this sequence is not corrupted by B_0 inhomogeneity effects. The FID signal was acquired from 11 to 70 μs at a sampling decay of 0.4 μs. For the CPMG measurements, the 90° to 180° pulse spacing was 0.1 ms and the signal of a single point at the echo maximum was acquired. Data were averaged over 64 acquisitions. The number of successive echoes recorded was adjusted for each sample according to its T2. The recycle delay for each sample was adjusted after measurement of the T1 with a fast saturation recovery sequence. The total time of acquisition of data for T2 (including spectrometer adjustments and T1 measurement) was about 10 min per sample.

Fitting was performed in two steps. First, T2 relaxation curves from the CPMG data only (after removing the FID signal from the combined FID-CPMG signal) were fitted by Scilab software according to the MEM (Mariette et al., 1996), which provides a continuous distribution of relaxation components without any assumption concerning their number. In this representation, the peaks of the distribution are centered at the corresponding most probable T2 values, while peak areas correspond to the intensity of the T2 components. Then, T2 relaxation curves obtained by the combined FID-CPMG sequence were also analyzed using the Levenberg-Marquardt algorithm, which allows a discrete solution for the complete fitting curve according to the equation:

$$I(t) = I_1 \exp(-t/T_{21})^2 + \sum_{i=2} I_{0i} \exp(-t/T_{2i}) + offset \quad (1)$$

where I_{0i} is the intensity of the i_{th} exponential at the equilibrium state and T_{2i} is the characteristic transverse relaxation time for the i_{th} exponential. The number of terms that best described the relaxation curve was determined by examining the residual plots and the values of the coefficient of determination.

Water Relations

The water relations were studied for all leaf samples examined by NMR. Leaf samples were weighed within the NMR tubes before (fresh weight) and after each NMR experiment in order to check possible water loss during the measurements. At the end of the NMR experiments, samples were transferred to laboratory cups and dried in an oven at 103°C for 24 h and weighed (dry weight). The water content (WC) was expressed as a percentage of fresh weight:

$$WC = (\text{fresh weight} - \text{dry weight})/\text{fresh weight} \quad (2)$$

Dry matter, fresh matter, and water masses were calculated on the basis of leaf area of the six leaf discs used. Specific LWW per component (LWW_i) was computed according to the equation:

$$LWW_i = \frac{I_{0i}\ x\ m_w}{A} \quad (3)$$

where m_w corresponds to water mass of the NMR sample made of six leaf discs in g, A to the area of the discs in m^2, and I_{0i} to the relative intensity of the i^{th} NMR signal component as a percentage.

RWC was measured as described by Turner et al. (2007). Leaf samples were placed in a vial, weighed, and then floated for 2 h on freshly distilled water at 4°C. The turgid weight was then determined. The sample was then oven dried at 70°C for 48 h and weighed. The RWC is then:

$$RWC = (\text{fresh weight} - \text{dry weight})/(\text{turgid weight} - \text{dry weight}) \quad (4)$$

Leaf water potential (Ψ_l) and leaf osmotic potential at that RWC (π_{RWC}) were measured as described previously (Leport et al., 1999).

The turgor pressure (T) was calculated as:

$$T = \Psi_l - \pi_{RWC} \quad (5)$$

The water deficit (WD) was calculated as:

$$WD = 1 - RWC. \quad (6)$$

Electron and Light Microscopy

Sample Preparation and Micrograph Acquisition

After sampling, the fixative solution (2% [w/v] paraformaldehyde and 2.5% [w/v] glutaraldehyde) was infiltrated into the leaf tissues using five cycles of depressurization with a vacuum pump (15 min of low pressure in each cycle). Samples were replaced in the same fixative solution for 24 h at 4°C. After extensive washing in 0.2 mol L^{-1} phosphate buffer (PB; pH 6.8), samples were incubated for 60 min in 2% (w/v) tannic acid solution in PB, washed in PB, and postfixed for 90 min with 2% (w/v) osmium tetroxide. Samples were then washed in PB and dehydrated in a graded series of increasing concentrations of ethanol (50%, 70%, 90%, and 100% [v/v]). Pure ethanol was then replaced by propylene oxide, and samples were gradually infiltrated with increasing concentrations (30%, 50%, 70%, and 100% [v/v]) of epoxy resin (mixed with propylene oxide) for a minimum of 3 h per step. Samples were left overnight in epoxy resin. Infiltration with DMP30-epoxy resin was continued the next day for 3 h. Samples were finally embedded in a new mix of DMP30-epoxy resin and polymerized at 60°C for 24 h.

For photonic microscopy, thin sections (500 nm) were cut with a Leica ultracut UCT ultramicrotome and stained with toluidine blue before they were observed with a Nikon Eclipse 80i microscope. For transmission electron microscopy analysis, ultrathin sections (80 nm) were then cut with a UCT Leica ultramicrotome, placed on grids poststained for 60 min with uranyl acetate and then for 20 min with lead citrate, and viewed with a JEOL 1400 transmission electron microscope supplied with a Gatan Orius camera.

Model

A simplified model similar to that employed by McCain (1995) was used to interpret microscope images. Our model took into account only the palisade layer and assumed it to be an ordered arrangement of water-filled cells with an ellipsoidal shape. It was also assumed that cell width was equal to cell depth, wall thickness was uniform over the cell, and chloroplasts covered all the inner surface of cell walls while the hyaloplasma contained a negligible water fraction of the cell. As the focus was on the layer that was most affected by senescence, where most of the chloroplasts can be found, the spongy layer was not taken into consideration.

An example of the optical microscope images used for the estimation of cell and vacuole dimensions is shown in Figure 10A. The optical microscope images were also used to measure the perimeter of the cell wall, and its thickness was estimated from electron micrographs (Fig. 10B).

The vacuole ($V_{VACUOLE}$), chloroplast ($V_{CHLOROPLAST}$), and wall (V_{WALL}) volumes were estimated using the model according to following equations:

$$V_{VACUOLE} = 3/4\pi \times 1/8 \times \left[W_V^2 \times L_V\right] \quad (7)$$

$$V_{CHLOROPLAST} = 3/4\pi \times 1/8 \times \left[\left(W_C^2 \times L_C\right) - \left(W_V^2 \times L_V\right)\right] \quad (8)$$

$$V_{WALL} = 3/4\pi \times 1/8 \times \left[\left((W_C + 2W_W)^2 \times (L_C + 2W_W)\right) - \left(W_C^2 \times L_C\right)\right] \quad (9)$$

where W_C is cell width, L_C is cell length, W_V is vacuole width, L_V is vacuole length, L_W is wall length, and W_W is wall thickness. W_C and L_C do not include the cell wall.

Microscopy images were analyzed using ImageJ software. The images were first manually segmented, and quantitative data related to cell structure were then extracted from the two youngest and the two most senescent leaves analyzed. Data were expressed as percentage of the total cell volume in order to compare the evolution of the relative volume of the different compartments with that of the intensity of the different NMR signal components.

Data Analyses

Correlation (PCA)

PCA, defined as an unsupervised descriptive multivariate statistics tool, was performed with R software, package FactomineR, on the 50 data sets from

11 plants (P-1, P-3, P-4, P-6, P-7, P-8, P-9, P-11, P-13, P-14, and P-15), consisting of the changes in 10 multivariate data of the six leaves at different leaf ranks (6–1). The multivariate data were as follows: chlorophyll, starch, and water content, dry matter, $T_{2(comp.1)}$, $T_{2(comp.3)}$, and $T_{2(comp.4+5)}$ [weighted average of $T_{2(comp.4)}$ and $T_{2(comp.5)}$], and $I_{0(comp.2)}$, $I_{0(comp.3)}$, and $I_{0(comp.\ 4+5)}$ corrected for the receiver gain and the sample weight.

ANOVA

ANOVA was performed using the software package Statgraphics Plus (Centurion) to detect significant differences ($P < 0.01$) between measurements on different leaf ranks. The one-factor ANOVA test was applied to the different leaf water status measurements. The multiple range Fisher LSD test was used to detect significant differences between groups.

ACKNOWLEDGMENTS

We thank Dominique Poulain (UMR SAS (Soil, Agro and hydroSystem), INRA Agrocampus Ouest) for help with the statistical analyses. We also thank the greenhouse team, particularly Laurent Charlon, Loic Daniel, and Patrick Rolland (all IGEPP). We acknowledge the Genetic Resource Center (BrACySol BRC, UMR IGEPP, INRA Ploudaniel, France) for providing the seeds of the Tenor variety. Finally, we thank Sophie Rolland for starch analysis, Anne-Marie Gouraud for molecular analysis, and Françoise Leprince and Patrick Leconte (all IGEPP) for sample processing.

Received June 10, 2013; accepted July 29, 2013; published July 31, 2013.

LITERATURE CITED

Adam Z, Clarke AK (2002) Cutting edge of chloroplast proteolysis. Trends Plant Sci **7:** 451–456

Albert B, Le Cahérec F, Niogret M-F, Faes P, Avice J-C, Leport L, Bouchereau A (2012) Nitrogen availability impacts oilseed rape (Brassica napus L.) plant water status and proline production efficiency under water-limited conditions. Planta **236:** 659–676

Bréhélin C, Kessler F, van Wijk KJ (2007) Plastoglobules: versatile lipoprotein particles in plastids. Trends Plant Sci **12:** 260–266

Buchanan-Wollaston V (1997) The molecular biology of leaf senescence. J Exp Bot **48:** 181–199

Buchanan-Wollaston V, Earl S, Harrison E, Mathas E, Navabpour S, Page T, Pink D (2003) The molecular analysis of leaf senescence: a genomics approach. Plant Biotechnol J **1:** 3–22

Capitani D, Brilli F, Mannina L, Proietti N, Loreto F (2009) In situ investigation of leaf water status by portable unilateral nuclear magnetic resonance. Plant Physiol **149:** 1638–1647

Cosgrove DJ (1993) Wall extensibility: its nature, measurement and relationship to plant cell growth. New Phytol **124:** 1–23

Cosgrove DJ (1999) Enzymes and other agents that enhance cell wall extensibility. Annu Rev Plant Physiol Plant Mol Biol **50:** 391–417

Desclos M, Dubousset L, Etienne P, Le Caherec F, Satoh H, Bonnefoy J, Ourry A, Avice J-C (2008) A proteomic profiling approach to reveal a novel role of *Brassica napus* drought 22 kD/water-soluble chlorophyll-binding protein in young leaves during nitrogen remobilization induced by stressful conditions. Plant Physiol **147:** 1830–1844

Diaz C, Lemaître T, Christ A, Azzopardi M, Kato Y, Sato F, Morot-Gaudry J-F, Le Dily F, Masclaux-Daubresse C (2008) Nitrogen recycling and remobilization are differentially controlled by leaf senescence and development stage in Arabidopsis under low nitrogen nutrition. Plant Physiol **147:** 1437–1449

Diaz C, Purdy S, Christ A, Morot-Gaudry JF, Wingler A, Masclaux-Daubresse CL (2005) Characterization of markers to determine the extent and variability of leaf senescence in Arabidopsis: a metabolic profiling approach. Plant Physiol **138:** 898–908

Dreccer MF, Schapendonk A, Slafer GA, Rabbinge R (2000) Comparative response of wheat and oilseed rape to nitrogen supply: absorption and utilisation efficiency of radiation and nitrogen during the reproductive stages determining yield. Plant Soil **220:** 189–205

Ellis JR, Leech RM (1985) Cell size and chloroplast size in relation to chloroplast replication in light-grown wheat leaves. Planta **165:** 120–125

Etienne P, Desclos M, Le Goua L, Gombert J, Bonnefoy J, Maurel K, Le Dily F, Ourry A, Avice J-C (2007) N-protein mobilisation associated with the leaf senescence process in oilseed rape is concomitant with the disappearance of trypsin inhibitor activity. Funct Plant Biol **34:** 895–906

Fischer AM (2007) Nutrient remobilization during leaf senescence. *In* S Gan, ed, Senescence Processes in Plants. Annual Plant Reviews, Vol 26. Blackwell Publishing, New York, pp 87–107

Franzaring J, Gensheimer G, Weller S, Schmid I, Fangmeier A (2012) Allocation and remobilisation of nitrogen in spring oilseed rape (Brassica napus L. cv. Mozart) as affected by N supply and elevated CO_2. Environ Exp Bot **83:** 12–22

Gombert J, Etienne P, Ourry A, Le Dily F (2006) The expression patterns of SAG12/Cab genes reveal the spatial and temporal progression of leaf senescence in Brassica napus L. with sensitivity to the environment. J Exp Bot **57:** 1949–1956

Gookin TE, Hunter DA, Reid MS (2003) Temporal analysis of alpha and beta-expansin expression during floral opening and senescence. Plant Sci **164:** 769–781

Guiboileau A, Yoshimoto K, Soulay F, Bataillé M-P, Avice J-C, Masclaux-Daubresse C (2012) Autophagy machinery controls nitrogen remobilization at the whole-plant level under both limiting and ample nitrate conditions in Arabidopsis. New Phytol **194:** 732–740

Hikosaka K (2005) Leaf canopy as a dynamic system: ecophysiology and optimality in leaf turnover. Ann Bot (Lond) **95:** 521–533

Hills BP, Duce SL (1990) The influence of chemical and diffusive exchange on water proton transverse relaxation in plant tissues. Magn Reson Imaging **8:** 321–331

Hills BP, Nott KP (1999) NMR studies of water compartmentation in carrot parenchyma tissue during drying and freezing. Appl Magn Reson **17:** 521–535

Hirel B, Le Gouis J, Ney B, Gallais A (2007) The challenge of improving nitrogen use efficiency in crop plants: towards a more central role for genetic variability and quantitative genetics within integrated approaches. J Exp Bot **58:** 2369–2387

Hoertensteiner S (2006) Chlorophyll degradation during senescence. Annu Rev Plant Biol **57:** 55–77

Honda SI, Hongladarom-Honda T, Kwanyuen P, Wildman SG (1971) Interpretations on chloroplast reproduction derived from correlations between cells and chloroplasts. Planta **97:** 1–15

Kaup MT, Froese CD, Thompson JE (2002) A role for diacylglycerol acyltransferase during leaf senescence. Plant Physiol **129:** 1616–1626

Keech O, Pesquet E, Ahad A, Askne A, Nordvall D, Vodnala SM, Tuominen H, Hurry V, Dizengremel P, Gardeström P (2007) The different fates of mitochondria and chloroplasts during dark-induced senescence in Arabidopsis leaves. Plant Cell Environ **30:** 1523–1534

Krupinska K, Humbeck K (2008) Senescence processes and their regulation. Plant Biol (Stuttg) (Suppl 1) **10:** 1–3

Lee RH, Wang CH, Huang LT, Chen SCG (2001) Leaf senescence in rice plants: cloning and characterization of senescence up-regulated genes. J Exp Bot **52:** 1117–1121

Lemaître T, Gaufichon L, Boutet-Mercey S, Christ A, Masclaux-Daubresse C (2008) Enzymatic and metabolic diagnostic of nitrogen deficiency in Arabidopsis thaliana Wassileskija accession. Plant Cell Physiol **49:** 1056–1065

Leport L, Turner NC, French RJ, Barr MD, Duda R, Daves SL, Tennant D, Siddique KHM (1999) Physiological responses of chickpea genotypes to terminal drought in a Mediterranean-type environment. Eur J Agron **11:** 279–291

Lim PO, Kim HJ, Nam HG (2007) Leaf senescence. Annu Rev Plant Biol **58:** 115–136

Maheswari M, Joshi DK, Saha R, Nagarajan S, Gambhir PN (1999) Transverse relaxation time of leaf water protons and membrane injury in wheat (Triticum aestivum L.) in response to high temperature. Ann Bot (Lond) **84:** 741–745

Malagoli P, Laine P, Rossato L, Ourry A (2005) Dynamics of nitrogen uptake and mobilization in field-grown winter oilseed rape (Brassica napus) from stem extension to harvest. I. Global N flows between vegetative and reproductive tissues in relation to leaf fall and their residual N. Ann Bot (Lond) **95:** 853–861

Mariette F, Brannelec C, Vitrac O, Bohuon P (1999) Effet du procédé de friture sur la répartition et l'état de l'eau mesurée par RMN et IRM. *In* Les Produits Alimentaires et l'Eau, Agoral 99. Edition Tec & Doc, Nantes, France, pp 411–416

Mariette F, Guillement JP, Tellier C, Marchal P (1996) Continuous relaxation time distribution decomposition by MEM. *In* DN Rutledge, ed,

Signal Treatment and Signal Analysis in NMR. Elsevier, Paris, pp 218–234

Marigheto NA, Moates GK, Furfaro ME, Waldron KW, Hills BP (2009) Characterisation of ripening and pressure-induced changes in tomato pericarp using NMR relaxometry. Appl Magn Reson **36:** 35–47

Martínez DE, Costa ML, Guiamet JJ (2008) Senescence-associated degradation of chloroplast proteins inside and outside the organelle. Plant Biol (Stuttg) (Suppl 1) **10:** 15–22

Masclaux C, Valadier MH, Brugière N, Morot-Gaudry JF, Hirel B (2000) Characterization of the sink/source transition in tobacco (Nicotiana tabacum L.) shoots in relation to nitrogen management and leaf senescence. Planta **211:** 510–518

Masclaux-Daubresse C, Reisdorf-Cren M, Orsel M (2008) Leaf nitrogen remobilisation for plant development and grain filling. Plant Biol (Stuttg) (Suppl 1) **10:** 23–36

McCain DC (1995) Nuclear magnetic resonance study of spin relaxation and magnetic field gradients in maple leaves. Biophys J **69:** 1111–1116

McIntyre GI (1987) The role of water in the regulation of plant development. Can J Bot **65:** 1287–1298

Mohapatra PK, Patro L, Raval MK, Ramaswamy NK, Biswal UC, Biswal B (2010) Senescence-induced loss in photosynthesis enhances cell wall beta-glucosidase activity. Physiol Plant **138:** 346–355

Oshita S, Maeda A, Kawagoe Y, Tsuchiya H, Kuroki S, Seo Y, Makino Y (2006) Change in diffusional water permeability of spinach leaf cell membrane determined by nuclear magnetic resonance relaxation time. Biosystems Eng **95:** 397–403

Otegui MS, Noh YS, Martínez DE, Vila Petroff MG, Staehelin LA, Amasino RM, Guiamet JJ (2005) Senescence-associated vacuoles with intense proteolytic activity develop in leaves of Arabidopsis and soybean. Plant J **41:** 831–844

Qiao Y, Galvosas P, Callaghan PT (2005) Diffusion correlation NMR spectroscopic study of anisotropic diffusion of water in plant tissues. Biophys J **89:** 2899–2905

Reid MS, Chen JC (2007) Flower senescence. *In* S Gan, ed, Senescence Processes in Plants. Annual Plant Reviews, Vol 26. Blackwell Publishing, New York, pp 256–277

Reviron MP, Vartanian N, Sallantin M, Huet JC, Pernollet JC, de Vienne D (1992) Characterization of a novel protein induced by progressive or rapid drought and salinity in *Brassica napus* leaves. Plant Physiol **100:** 1486–1493

Sibgatullin TA, Anisimov AV, de Jager PA, Vergeldt FJ, Gerkema E, Van As H (2007) [Analysis of diffusion and relaxation behavior of water in apple parenchymal cells]. Biofizika **52:** 268–276

Smith AM, Zeeman SC (2006) Quantification of starch in plant tissues. Nat Protoc **1:** 1342–1345

Snaar JEM, Van As H (1992) Probing water compartments and membrane permeability in plant cells by ^{1}H NMR relaxation measurements. Biophys J **63:** 1654–1658

Tang HR, Godward J, Hills B (2000) The distribution of water in native starch granules: a multinuclear NMR study. Carbohydr Polym **43:** 375–387

Teixeira RT, Knorpp C, Glimelius K (2005) Modified sucrose, starch, and ATP levels in two alloplasmic male-sterile lines of B. napus. J Exp Bot **56:** 1245–1253

Thomas H, Stoddart JL (1980) Leaf senescence. Annu Rev Plant Physiol Plant Mol Biol **31:** 83–111

Turner NC, Abbo S, Berger JD, Chaturvedi SK, French RJ, Ludwig C, Mannur DM, Singh SJ, Yadava HS (2007) Osmotic adjustment in chickpea (Cicer arietinum L.) results in no yield benefit under terminal drought. J Exp Bot **58:** 187–194

Van As H (1992) NMR in horticulture: in situ plant water balance studies with NMR. Acta Hortic **304:** 103-112

Van As H (2007) Intact plant MRI for the study of cell water relations, membrane permeability, cell-to-cell and long distance water transport. J Exp Bot **58:** 743–756

Van der Weerd L, Claessens M, Efde C, Van As H (2002) Nuclear magnetic resonance imaging of membrane permeability changes in plants during osmotic stress. Plant Cell Environ **25:** 1539–1549

Verwoerd TC, Dekker BMM, Hoekema A (1989). A small-scale procedure for the rapid isolation of plant RNAs. Nucleic Acids Res **17:** 2362.

Wada S, Ishida H, Izumi M, Yoshimoto K, Ohsumi Y, Mae T, Makino A (2009) Autophagy plays a role in chloroplast degradation during senescence in individually darkened leaves. Plant Physiol **149:** 885–893

Wingler A, Mares M, Pourtau N (2004) Spatial patterns and metabolic regulation of photosynthetic parameters during leaf senescence. New Phytol **161:** 781–789

Zellnig G, Perktold A, Zechmann B (2010) Fine structural quantification of drought-stressed Picea abies (L.) organelles based on 3D reconstructions. Protoplasma **243:** 129–136

Zhang M-P, Zhang C-J, Yu G-H, Jiang Y-Z, Strasser RJ, Yuan Z-Y, Yang X-S, Chen G-X (2010) Changes in chloroplast ultrastructure, fatty acid components of thylakoid membrane and chlorophyll a fluorescence transient in flag leaves of a super-high-yield hybrid rice and its parents during the reproductive stage. J Plant Physiol **167:** 277–285